



OPEN

Effect of mass disorder on the lattice thermal conductivity of MgO periclase under pressure

SUBJECT AREAS:

PHASE TRANSITIONS
AND CRITICAL
PHENOMENAGEODYNAMICS
MINERALOGY

CONDENSED-MATTER PHYSICS

Douglas Allen Dalton¹, Wen-Pin Hsieh^{2*}, Gregory T. Hohensee², David G. Cahill²
& Alexander F. Goncharov¹¹Geophysical Laboratory, Carnegie Institution of Washington, Washington, DC, ²Department of Materials Science and Engineering and Frederick Seitz Materials Research Laboratory, University of Illinois, Urbana, IL.Received
7 June 2013Accepted
24 July 2013Published
9 August 2013Correspondence and
requests for materials
should be addressed to
A.F.G. (goncharov@
gl.ciw.edu)* Current address:
Stanford Institute for
Materials and Energy
Sciences, Stanford
University and SLAC
National Accelerator
Laboratory, Menlo
Park, CA.

Thermal conductivity of mantle materials controlling the heat balance and thermal evolution of the Earth remains poorly constrained as the available experimental and theoretical techniques are limited in probing minerals under the relevant conditions. We report measurements of thermal conductivity of MgO at high pressure up to 60 GPa and 300 K via diamond anvil cells using the time-domain thermoreflectance technique. These measurements are complemented by model calculations which take into account the effect of temperature and mass disorder of materials within the Earth. Our model calculations agree with the experimental pressure dependencies at 300 and 2000 K for MgO. Furthermore, they predict substantially smaller pressure dependence for mass disordered materials as the mechanism of scattering changes. The calculated thermal conductivity at the core-mantle boundary is smaller than the majority of previous predictions resulting in an estimated total heat flux of 10.4 TW, which is consistent with modern geomodeling estimates.

Recently, there has been a great deal of experimental and theoretical activity in determining heat transport properties of the mantle minerals^{1–6} as these parameters have been realized to be critically important for geomodels aiming to better understand the Earth's thermal history and geodynamics^{7–9}. Central to this knowledge is the determination of various energy contributions to the Earth's overall energy balance. These can be estimated based on heat flow across the most distinct physical and chemical planetary interfaces --the Earth's surface, which is well constrained and the core-mantle boundary (CMB), which remains to be more precisely determined¹⁰. Knowledge of the overall energy balance gives access to various phenomena within Earth's interior such as radiogenic heating, dynamics of thermal plumes in the mantle, and also to the Earth's history, in particular to the extent to which deep mantle melting previously occurred¹¹.

Earth's mantle consists of simple and ternary (perovskite) oxides of Mg, Si, and Ca doped with Fe and Al. These materials are electrically insulating, thus thermal transport is governed by phonons. Other contributions to the heat transport, including radiative conductivity and convection, are not considered in this paper. Perovskite, (Mg,Fe)SiO₃, is the primary component within the Earth's mantle, while ferropericlase (Fe,Mg)O is the second most abundant mineral in the mantle. The experimental determinations of the lattice thermal conductivities of these materials are numerous^{1,5,12–15}, but limited in pressure and temperature and also in experimental accuracy. Thus, estimates of the thermal conductivity at the conditions of the CMB are based on phenomenological extrapolations^{16,17} and on theoretical first-principle calculations^{1,2,4,18–20}, both of which are not validated experimentally. Moreover, since the major mantle minerals are solid solutions and have mass disorder, their thermal conductivity is greatly affected²¹. This effect has been theoretically estimated in the case of isotopic substitution¹⁹, but has not been examined for large mass disorder in mixed crystals such as ferropericlase. Until now, the effect of mass disorder could only be estimated through experimental investigations that were limited to low pressure¹. Pressure dependence of thermal conductivity in the case of disordered materials has never been addressed.

Here we present data on the thermal conductivity of MgO - a prototype oxide- up to 60 GPa to establish a baseline for the pressure dependence of thermal conductivity. We used the time domain thermoreflectance technique^{22,23}, which offers a non-contact, optical method for extending thermal transport measurements of mantle materials to higher pressure and temperature. To account for mass disorder and the effects of elevated temperature, we applied a Debye-Callaway-Morelli (DCM) model²⁴, which closely described the experimental



results for the ordered material, while predicted substantially lower pressure dependencies for the mass disordered materials. These results allowed us to perform more robust extrapolations of available experimental data to the CMB conditions, yielding a value of 10.4 TW for the heat transport through the CMB, thus supporting the latest geomodeling results.

Results

Figure 1 shows example data for the in-phase (V_{in}) and ratio ($-V_{in}/V_{out}$) signals of the TDTR measurements on the MgO coated with Al film at ambient condition. The thermal conductivity of MgO was determined by comparing the ratio $-V_{in}/V_{out}$ as a function of delay time with the calculation of a thermal model that takes into account the heat flow into the MgO substrate as well as the heat flow into the Ar medium^{25–27}. Since the thermal penetration depth in MgO at the modulation frequency of pump beam (10 MHz) is ~ 0.7 – 1.2 μm , small compared to the radius of the laser spot size, ~ 7.5 μm , the heat flow in our sample geometry is predominantly one-dimensional. The parameters of the thermal conductivity model are given in supplementary materials.

The DCM model²⁴, which we have used to calculate the effects of mass disorder and temperature effects, is derived from the Boltzmann transport equation²⁸ for an isotropic and linear phonon

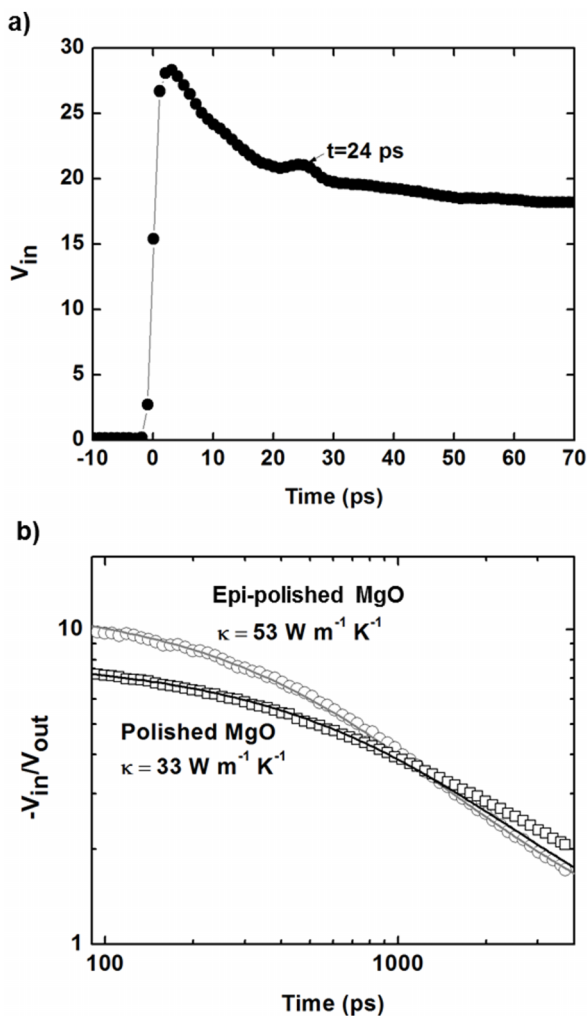


Figure 1 | Ambient pressure data: (a) In-phase (V_{in}) signal as a function of time. The metallic transducer film thickness can be determined from the acoustic echo signal which is present within the V_{in} signal. (b) Ratio ($-V_{in}/V_{out}$) signal as a function of time for epi-polished and hand polished MgO, along with fit to the thermal calculation.

dispersion, and assumes functional forms for the normal and resistive phonon relaxation rates for the longitudinal and transverse modes. For each mode we assume a truncated Debye dispersion, with cutoff frequency set by the acoustic phonon frequency near the [100] zone edge as a linear function of MgO density (see Ref. 2, Suppl. Materials). As such, this calculated κ_{DCM} includes only acoustic modes, so to account for the optical modes our model is actually $\kappa_{\text{MgO}} = \kappa_{\text{DCM}} + \kappa_{\text{min}}$, where κ_{min} is the minimum thermal conductivity (in the limit of an amorphous solid) from Ref. 29. Further details of our DCM model are given in supplementary materials.

We begin with the description of the experimental results for periclase. Two experimental runs to 32 and 59 GPa yielded consistent data sets. Figure 2 shows the high pressure thermal conductivity data up to pressures of 60 GPa compared to various phenomenological models for predicting the high pressure behavior of MgO. The ambient pressure thermal conductivity value (53(2) W/m/K) is in agreement with that found in literature³⁰, which showed single crystal MgO at 298 K in air to have a mean value of 55.2 ± 0.4 W/m/K. The experimental error bars determine the uncertainty of the fit to the experimental time series (Fig. 1) vary from 10% at low to 19% at high pressures. These uncertainties are comparable to those of the classical Angstrom method for the large press measurements^{1,2} and are better than those which have been reported recently by thermo-reflectance on the ns time scale⁵.

Our high-pressure data for the thermal conductivity, κ can be fit well by a linear function (Fig. 2), but can also be fit linearly on a log-log scale as a function of density (inset). This is useful in comparing with phenomenological descriptions, which usually assume the power law dependence as a function of density and temperature,

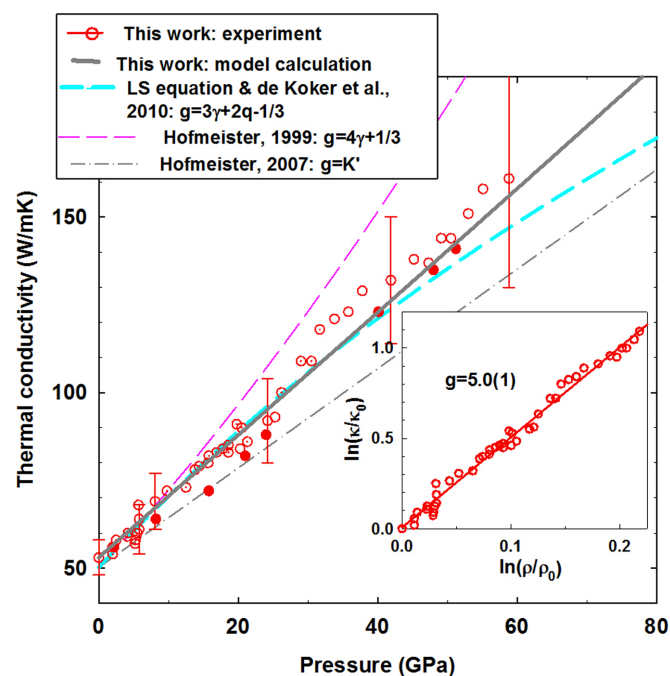


Figure 2 | Thermal conductivity of MgO up to 60 GPa at room temperature. The open and dotted circles are our data on pressure increase for two different pressure runs; the filled circles are our data on pressure release. The inset shows the data plotted in a log-log scale; the solid curve is the linear fit. Gray thick line is the results of the DCM calculations from this work. Phenomenological predictions are shown by the long dashed line¹⁶, dashed-dotted line¹⁶, and short dashed line². The latter description coincides with that determined from the Leibfried-Schlömann equation³² $\kappa = AV^{1/3}\omega_D^3\gamma^{-2}T^{-1}$, where V is volume, ω_D is Debye frequency, γ is the Grüneisen parameter, T is temperature and A serves as a fit parameter.



Table 1 | Parameters used in phenomenological calculations of thermal conductivity in Fig. 2

Model	γ	q	κ_0	K	K'	G	κ
Hofmeister, $g = 4\gamma + 1/3$	1.54	-	50.2	157.37	4.44	$4\gamma + 1/3$	$\kappa_0(1 + K'P/K)^{g/K}$
Hofmeister, $g = K'$	1.54	-	50.2	157.37	4.44	K'	$\kappa_0(1 + K'P/K)^{g/K}$
De Koker	1.49	1.27	50.2	-	-	$3\gamma + 2q - 1/3$	$\kappa_0(\rho/3.583)^g$

$$\kappa = \kappa_0 \left(\frac{\rho}{\rho_0} \right)^g \left(\frac{T_0}{T} \right)^\beta \quad (1)$$

where zero subscript refers to the reference density ρ and temperature T (here ambient P and T) and g and β are the power coefficients, which are assumed to be P - T independent.

One can see that our data differ from the most common phenomenological predictions for the pressure dependence of the thermal conductivity. These are based on the Debye approximation and consider three-phonon scattering by acoustic phonons as the dominant carrier. The relevant model parameters include the Gruneisen parameter, γ , its logarithmic volume derivative, q , the bulk modulus K , and its pressure derivative K' . All these parameters have been accurately determined experimentally at ambient pressure (Table 1), justifying the comparison with the experimental data presented here (Fig. 2). Notably, the initial logarithmic derivatives of κ are within 10% of the models presented in Refs. 31 and 2 (2.1%/GPa vs 1.9%/GPa by our determination).

Some of the results diverge substantially at higher pressures, demanding better description under conditions approaching those of the deep Earth's mantle. We also find that the results of phenomenological predictions depend on the thermodynamic model chosen, as the parameter g in equation (1) can be pressure dependent in some models. Use of the self-consistent thermodynamic models^{1,2} gives a good description of the experimental data (Fig. 3). In this case the parameter g was determined using the Debye theory² $g = 3\gamma + 2q - 1/3$. The Leibfreid-Schlomann (LS) equation $\kappa = A \frac{V^{1/3} \omega_D^3}{\gamma^2 T}$ ³² is essentially equivalent to the Eq. (1) with g determined using the same expression. The results of our DCM calculations at 300 K for pure MgO agree well with experimental pressure dependence.

It is also instructive to compare our data with the first-principles theoretical calculations (Fig. 3). For the first-principles calculations, the values of the thermal conductivity at ambient conditions spread over a large range of 65–111 W m⁻¹ K⁻¹ (see Table 1 in Ref. 3), but these determinations were performed for a perfect, isotopically pure crystal, which overestimate the thermal conductivity value compared to that with natural isotope composition by nearly 50%¹⁹. The theoretical data presented in Fig. 3 except that of Ref. 4 have been normalized to our experimental value at ambient pressure as they differ substantially. Since the data of Ref. 4 represent the results for the ideal, isotopically pure material, they require the correction, making good agreement with the experimental observations coincidental. As one can see, most calculations agree well with our data in the pressure range of the experimental data; however, using the extrapolation of these calculations to the pressure range of the lower interior requires caution. We conclude the description of the room temperature data by stating that the absolute majority of the previously reported phenomenological and first-principle calculations were not able to predict the correct value of the thermal conductivity and its pressure dependence of such archetypal material as periclase mineral up to the lower mantle conditions.

We move now to high-temperature data, which are of particular interest in the geosciences. We will analyze the available data on the thermal conductivity of MgO at 2000 K, as this temperature is in the proximity to the conditions of the geotherm in the lower mantle (Fig. 4). The available experimental data for pure MgO^{1,12,33} are in

fair agreement, although the large uncertainty does not allow us to confidently extend the pressure dependence of thermal conductivity to the conditions approaching those at the CMB. First-principles calculations show a large spread above 40 GPa^{1,3,4,19}. Our DCM calculations match well with the experimental data and agree with some first-principles calculations⁴.

The next step is to evaluate the effect of mass disorder caused by atomic substitutions in deep Earth minerals. Manthilake et al.¹ performed so far the only experiment which shed some light on this problem. Their data on ferroperoclase at 14 GPa shown in Fig. 4 show a drastic decrease of the thermal conductivity due to Fe substitution. They also proposed a model based on the results of calculations for pure MgO to extrapolate the results to high pressures. Our DCM calculations for the mass disordered material at 2000 K are in proximity of their results, but propose much weaker pressure dependence relative to that of pure MgO.

Discussion

In pure MgO, the dominant phonon scattering mechanism is three-phonon scattering due to anharmonicity. In ferropericlase, three-phonon scattering dominates at low frequencies and mass-disorder at high frequencies, altering the dependence of κ on P and T . When mass disorder is important, Klemens³⁴ predicts a temperature dependence of $T^{-1/2}$ instead of the more typical T^{-1} dependence of pure crystals. Manthilake et al.¹ also found a decrease in the temperature power parameter from 0.76 for MgO to 0.24 for Mg_{0.8}Fe_{0.2}O and Mg_{0.95}Fe_{0.05}O. However, they used the same power parameter for the pressure dependence. Following the predictions of the LS

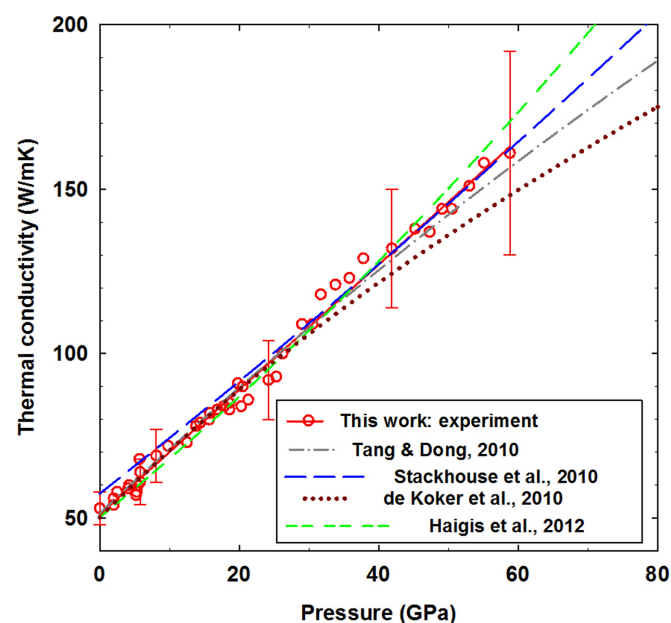


Figure 3 | Thermal conductivity of MgO up to 60 GPa at room temperature. The open circles are our data; the solid curve is the linear fit. The results of first-principle theoretical calculations are shown by lines of different styles. Dotted-dashed line- Ref. 19, long dashed line- Ref. 4, dotted line- Ref. 2, short dashed line-Ref. 3. The results are scaled to match the experimental value at 0 GPa for all calculations except that from Ref. 4.

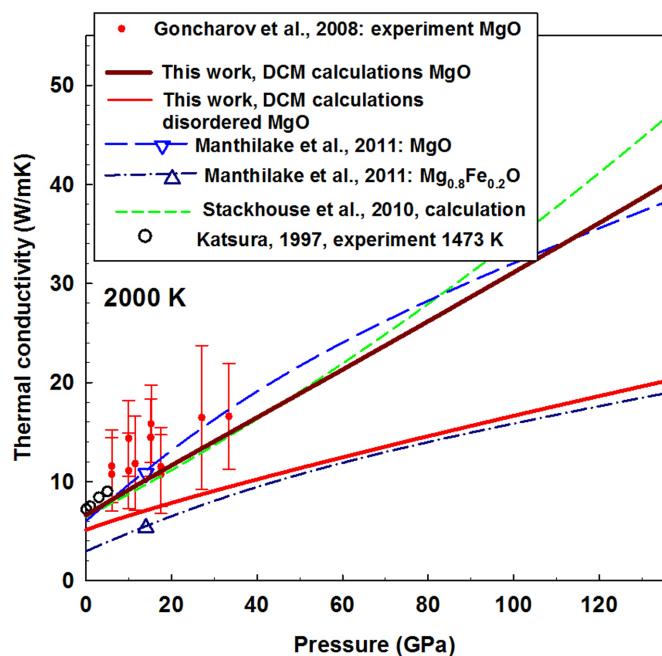


Figure 4 | Thermal conductivity of MgO at 2000 K up to 135 GPa. The closed circles with large error bars are experimental data from Ref. 34, the open circles are experimental data of Katsura at 1473 K¹². The reliable extrapolation of these data to 2000 K cannot be done. Open triangles up and down are extrapolations to 2000 K of the experimental data obtained up to 1273 K for MgO and Mg_{0.8}Fe_{0.2}O, respectively, from Ref. 1. The results of our DCM calculations are shown in thick solid line for pure MgO and thin solid line - for mass disordered MgO ($\gamma = 0.1$). The results of first-principle theoretical calculations for MgO are shown by lines of different styles: short dashed line- Ref. 4, long dashed line- Ref. 1.

equation, we argue that κ scaling as ω_D^3 for pure material (which works reasonably well- see Fig. 3) should change in materials with strong mass disorder to ω_D^2 , that is $\kappa \propto \omega_D^2 T^{-1/2}$. Use of this equation predicts weaker pressure dependence for the materials with mass disorder. Our DCM calculations for mass disordered MgO shows much weaker pressure dependence of the thermal conductivity (Fig. 4), which can be approximated by Eq. (1) with $g = 3.0$.

Our findings warrant a new estimation of the thermal conductivity at the CMB. For the thermal conductivity of ferropericlase, we used a value determined in our DCM calculations scaled to higher temperature using $T^{-0.241}$ dependence. This yields the values of 19 and 17.1 W/m/K at the top and bottom of the boundary layer², respectively. For iron-bearing magnesium silicate perovskite, we estimated the thermal conductivity based on the direct measurements of Mg_{0.97}Fe_{0.03}SiO₃¹ using Eq. (1) with $g = 3.0$ (our DCM calculations) and $\beta = 0.2^1$. This yielded 6.7 and 6.1 W/m/K at the top and the bottom of the boundary layer, respectively. Using the Hashin-Shtrikman aggregate averaging and assuming a two-component boundary layer, we obtain the thermal conductivity values at the top and the bottom of the boundary layer to be, respectively, 8.5 and 7.7 W/m/K. The estimated heat flux through the CMB is about 10.4 TW, which is consistent with previous estimations based on geophysical arguments¹⁰. This value, is in line with previous estimates based on measurements or theoretical calculations of the thermal conductivity^{1,3,5,6}, except the results of de Koker². In this latter work, De Koker greatly underestimated the value of the thermal conductivity for the perovskite phase by using the results of material with different chemical composition. Our small flux value due to the lattice conductivity cannot be adjusted substantially due to low radiative conductivity of perovskite³³ (cf., see a conflicting report from Ref. 35). The presence of the post-perovskite phase should increase

the lattice conductivity (e.g., Ref. 3), but the radiative component diminishes¹³.

We have presented measurements of thermal conductivity for MgO up to pressures of 60 GPa within a DAC using an all-optical pump-probe technique at ambient temperature. The pressure dependence for the thermal conductivity of MgO was found to obey the power law of density with the power parameter g of 5.0(1), corresponding to an isothermal pressure coefficient of 2.1% GPa⁻¹. We have also performed DCM calculations of the pressure dependence of pure and mass disordered MgO at 300 and 2000 K. The results show that mass disorder substantially reduces the value and the pressure dependence of the thermal conductivity. Using these results as a guide, we revisited the estimations of the heat flux through the CMB by extrapolating the pressure dependencies of the thermal conductivities of mass disordered mantle minerals to CMB conditions. The result for the heat flux agrees with the majority of the previous estimates and lies in the middle of the current geophysical estimations. Future more careful estimations of the heat transport properties of deep Earth will require verification of the results of the calculations presented here.

Methods

Samples of (100) orientation MgO (SPI supplies) had a polish that is suitable for the epitaxial growth of other materials on the MgO as a substrate (epi-polished). They were heated to 1200 K for 15–30 minutes under vacuum to remove hydroxides and other volatile hydrocarbons from the exposed MgO surface. The substrates of MgO were then coated *in situ* with ~ 80 nm Al film via magnetron sputtering. The back-side surface of the MgO (which was not coated) was then ground and polished to ~ 10 μm thickness and cleaved to 50×50 μm^2 pieces for sample loading into a symmetric piston-cylinder diamond anvil cell. The sample and a ruby ball were loaded into the cell with Ar as the pressure medium, so the Al film is sandwiched between the MgO sample and the Ar medium (Fig. 1S of supplementary materials).

The thermal conductivity of MgO at room temperature was measured by time domain thermoreflectance (TDTR), which utilizes sub-picosecond optical pulses to pump and probe the dynamics of thermal diffusion³⁶. In TDTR, the output of a mode-locked Ti:Sapphire oscillator was split into pump and probe beams: the pump beam heats the Al surface and the probe beam subsequently monitors changes in the optical reflectivity of Al due to the temperature evolution. The in-phase (V_{in}) and out-of-phase (V_{out}) signals of the variation of the reflected probe beam was then measured by a Si photodiode and an rf lock-in amplifier. The details of our TDTR system are outlined elsewhere³⁷.

1. Manthilake, G. M., de Koker, N., Frost, D. J. & McCammon, C. A. Lattice thermal conductivity of lower mantle minerals and heat flux from Earth's core. *Proceedings of the National Academy of Sciences* **108**, 17901–17904, doi:10.1073/pnas.1110594108 (2011).
2. de Koker, N. Thermal conductivity of MgO periclase at high pressure: Implications for the D' region. *Earth Planet Sc Lett* **292**, 392–398 (2010).
3. Haigis, V., Salanne, M. & Jahn, S. Thermal conductivity of MgO, MgSiO₃ perovskite and post-perovskite in the Earth's deep mantle. *Earth Planet Sc Lett* **355–356**, 102–108 (2012).
4. Stackhouse, S., Stixrude, L. & Karki, B. B. Thermal Conductivity of Periclase (MgO) from First Principles. *Phys Rev Lett* **104**, 208501 (2010).
5. Ohta, K. *et al.* Lattice thermal conductivity of MgSiO₃ perovskite and post-perovskite at the core–mantle boundary. *Earth Planet Sc Lett* **349–350**, 109–115 (2012).
6. Dekura, H., Tsuchiya, T. & Tsuchiya, J. Ab initio Lattice Thermal Conductivity of MgSiO₃ Perovskite as Found in Earth's Lower Mantle. *Phys Rev Lett* **110**, 025904, doi:Artn 025904 Doi 10.1103/Physrevlett.110.025904 (2013).
7. van den Berg, A. P., Rainey, E. S. G. & Yuen, D. A. The combined influences of variable thermal conductivity, temperature- and pressure-dependent viscosity and core-mantle coupling on the thermal evolution. *Phys Earth Planet In* **149**, 259–278, doi:DOI 10.1016/j.pepi.2004.10.008 (2005).
8. Tosi, N., Yuen, D. A. & Cadec, O. Dynamical consequences in the lower mantle with the post-perovskite phase change and strongly depth-dependent thermodynamic and transport properties. *Earth Planet Sc Lett* **298**, 229–243, doi:DOI 10.1016/j.epsl.2010.08.001 (2010).
9. Naliboff, J. B. & Kellogg, L. H. Dynamic effects of a step-wise increase in thermal conductivity and viscosity in the lowermost mantle. *Geophys Res Lett* **33**, L12S09, doi:Artn L12S09 Doi 10.1029/2006gl025717 (2006).
10. Lay, T., Hernlund, J. & Buffett, B. A. Core-mantle boundary heat flow. *Nature Geosci* **1**, 25–32 (2008).
11. Labrosse, S., Hernlund, J. W. & Coltice, N. A crystallizing dense magma ocean at the base of the Earth's mantle. *Nature* **450**, 866–869, doi:http://www.nature.com/nature/journal/v450/n7171/supplinfo/nature06355_S1.html. (2007).



12. Katsura, T. Thermal diffusivity of periclase at high temperatures and high pressures. *Phys Earth Planet In* **101**, 73–77 (1997).
13. Goncharov, A. F. *et al.* Effect of composition, structure, and spin state on the thermal conductivity of the Earth's lower mantle. *Phys Earth Planet In* **180**, 148–153, doi:http://dx.doi.org/10.1016/j.pepi.2010.02.002 (2010).
14. Goncharov, A. F., Beck, P., Struzhkin, V. V., Haugen, B. D. & Jacobsen, S. D. Thermal conductivity of lower-mantle minerals. *Phys Earth Planet In* **174**, 24–32 (2009).
15. Osako, M. & Ito, E. Thermal diffusivity of MgSiO₃ perovskite. *Geophys. Res. Lett.* **18**, 239–242, doi:10.1029/91gl00212 (1991).
16. Hofmeister, A. M. Pressure dependence of thermal transport properties. *Proceedings of the National Academy of Sciences* **104**, 9192–9197, doi:10.1073/pnas.0610734104 (2007).
17. Manga, M. & Jeanloz, R. Thermal conductivity of corundum and periclase and implications for the lower mantle. *J. Geophys. Res.* **102**, 2999–3008, doi:10.1029/96jb02696 (1997).
18. Cohen, R. E. Thermal Conductivity of MgO at High Pressures. *THE REVIEW OF HIGH PRESSURE SCIENCE AND TECHNOLOGY* **7**, 160–162 (1998).
19. Tang, X. & Dong, J. Lattice thermal conductivity of MgO at conditions of Earth's interior. *Proceedings of the National Academy of Sciences* **107**, 4539–4543 (2010).
20. de Koker, N. Thermal Conductivity of MgO Periclase from Equilibrium First Principles Molecular Dynamics. *Phys Rev Lett* **103**, 125902 (2009).
21. Klemens, P. G. The Scattering of Low-Frequency Lattice Waves by Static Imperfections. *P Phys Soc Lond A* **68**, 1113–1128, doi:Doi 10.1088/0370-1298/68/12/303 (1955).
22. Chen, B., Hsieh, W.-P., Cahill, D. G., Trinkle, D. R. & Li, J. Thermal conductivity of compressed H₂O to 22 GPa: A test of the Leibfried-Schlömann equation. *Phys Rev B* **83**, 132301 (2011).
23. Hsieh, W.-P., Chen, B., Li, J., Koblinski, P. & Cahill, D. G. Pressure tuning of the thermal conductivity of the layered muscovite crystal. *Phys Rev B* **80**, 180302 (2009).
24. Morelli, D. T., Heremans, J. P. & Slack, G. A. Estimation of the isotope effect on the lattice thermal conductivity of group IV and group III-V semiconductors. *Phys Rev B* **66**, 195304 (2002).
25. Feldman, A. Algorithm for solutions of the thermal diffusion equation in a stratified medium with a modulated heating source. *High Temperature-High Pressures* **31**, 293 (1999).
26. Cahill, D. Analysis of heat flow in layered structures for time-domain thermoreflectance. *Rev. Sci. Instrum.* **75** (2004).
27. Ge, Z., Cahill, D. G. & Braun, P. V. Thermal Conductance of Hydrophilic and Hydrophobic Interfaces. *Phys Rev Lett* **96**, 186101 (2006).
28. Callaway, J. Model for Lattice Thermal Conductivity at Low Temperatures. *Phys Rev* **113**, 1046–1051, doi:DOI 10.1103/PhysRev.113.1046 (1959).
29. Cahill, D., Watson, S. K. & Pohl, R. O. Lower limit to the thermal conductivity of disordered crystals. *Phys Rev B* **46**, 6131–6140 (1992).
30. Andersson, S. & Backstrom, G. Techniques for determining thermal conductivity and heat capacity under hydrostatic pressure. *Review of Scientific Instruments* **57**, 1633–1639 (1986).
31. Hofmeister, A. M. Mantle Values of Thermal Conductivity and the Geotherm from Phonon Lifetimes. *Science* **283**, 1699–1706 (1999).
32. Slack, G. A. in *Solid State Physics* Vol. Volume 34 (eds Frederick Seitz Henry Ehrenreich & Turnbull David) 1–71 (Academic Press, 1979).
33. Goncharov, A. F., Haugen, B. D., Struzhkin, V. V., Beck, P. & Jacobsen, S. D. Radiative conductivity in the Earth's lower mantle. *Nature* **456**, 231–234, doi:http://www.nature.com/nature/journal/v456/n7219/supinfo/nature07412_S1.html. (2008).
34. Klemens, P. G., White, G. K. & Tainsh, R. J. Scattering of lattice waves by point defects. *Philosophical Magazine* **7**, 1323–1335, doi:10.1080/14786436208213166 (1962).
35. Keppeler, H., Dubrovinsky, L. S., Narygina, O. & Kantor, I. Optical Absorption and Radiative Thermal Conductivity of Silicate Perovskite to 125 Gigapascals. *Science* **322**, 1529–1532, doi:10.1126/science.1164609 (2008).
36. Paddock, C. A. & Eesley, G. L. Transient thermoreflectance from thin metal films. *J Appl Phys* **60**, 285–290 (1986).
37. Kang, K., Koh, Y. K., Chiritescu, C., Zheng, X. & Cahill, D. G. Two-tint pump-probe measurements using a femtosecond laser oscillator and sharp-edged optical filters. *Rev. Sci. Instrum.* **79**, 114901 (2008).

Acknowledgments

D.A.D. and A.F.G. would like to acknowledge support from NSF EAR 1015239, CDAC and EFree. W.P.H., G.T.H. and D.G.C. would like to acknowledge support from the Carnegie-DOE Alliance Center (CDAC) through Grant No. DE-FC52-08NA28554.

Author contributions

A.F.G. and D.G.C. designed research. D.A.D., W.P.H. and A.F.G. conducted the experiments, G.T.H. and D.G.C. developed the mass disorder model. D.A.D., W.P.H., A.F.G. and G.T.H. wrote a manuscript. All authors reviewed the manuscript.

Additional information

Supplementary information accompanies this paper at <http://www.nature.com/scientificreports>

Competing financial interests: The authors declare no competing financial interests.

How to cite this article: Dalton, D.A., Hsieh, W.-P., Hohensee, G.T., Cahill, D.G. & Goncharov, A.F. Effect of mass disorder on the lattice thermal conductivity of MgO periclase under pressure. *Sci. Rep.* **3**, 2400; DOI:10.1038/srep02400 (2013).



This work is licensed under a Creative Commons Attribution-NonCommercial-NoDerivs 3.0 Unported license. To view a copy of this license, visit <http://creativecommons.org/licenses/by-nc-nd/3.0>